Fluid Mechanics and Mass Transfer in Melt Crystal Growth: Analysis of the Floating Zone and Vertical Bridgman Processes

Principal Investigator: Professor R.A. Brown

MV-70050

Summary

Fundamental understanding of the interactions of heat and mass transport, melt flow and the morphology of solidification interfaces are crucial to the design and interpretation of experiments aimed at microscopically controlled solidification of crystals on earth and in space. This research program focuses on analyses of the transport mechanisms in solidification processes, especially one of interest to the Microgravity Sciences and Applications Program of NASA. Research during the last year has focused on analysis of the dynamics of the floating zone process for growth of small-scale crystals, on studies of the effect of applied magnetic fields on convection and solute segregation in directional solidification, and on the dynamics of microscopic cell formation in two-dimensional solidification of binary alloys. The most significant findings have been:

1. The completion of the modification of our finite-element analysis of the thermal-capillary model for small-scale floating zones to include axisymmetric fluid flow in the melt driven by buoyancy differences, surface tension gradient and rotation of the feed and crystal rods.

2. Analysis of the effect of a vertically aligned applied magnetic field on buoyancy-driven convection and solute segregation in vertical directional solidification. Results are reported for specific crystal growth systems developed at MIT and Grenoble.

3. A study of the existence of a fundamental mechanism for wavelength selection in solidification of two-dimensional cellular interfaces from a binary melt based on large-scale numerical simulations has shown that steadily solidifying structures are possible for a **continuous range of wavelengths.** This results opposed results of model calculations for more idealized solidification systems where mechanisms for selecting a specific wavelength of the microstructure seem to exist.

4. The design and construction of an experimental system for the growth of two-dimensional microstructures is just about complete. This system is carefully designed for controlled, quantitative experimental measurements of interface morphologies over a range of operating conditions where theoretical predictions are available from our calculations.

Effect of Vertical Magnetic Field on Vertical Bridgman Crystal Growth

The successful prediction of interface morphologies and segregation in crystals grown by directional solidification involves complete solution of the macroscopic free-boundary problems that describe melt and heat flow, solute transfer and the melt/crystal interface morphology with accurate accounting of realistic heat transfer conditions for the particular furnace design. We have designed a numerical simulator for this purpose based on finite-element algorithms. Calculations from the simulations have been compared directly with experimental measurements for gallium-doped germanium growth in the apparatus built by A.F. Witt and MIT.[13] The agreement is remarkable, considering that no attempt has been made to adjust any of the thermo-physical properties. This work was highlighted in the 1985 annual report. In the last year we have extended the calculations in several ways. First we have incorporated the effect of an imposed axial magnetic field into the calculations to give accurate predictions of the intensity of the field needed to yield diffusion-controlled crystal growth on earth; this research has been submitted for publication and is highlighted below. Secondly, we have extended the finite-element simulations of directional solidification to include the transients associated with the batchwise nature of the system by solution of the time-dependent field equations and boundary conditions for the appropriate moving-boundary problem. The computer code for this effort is in the final stages of development and we will report in simulations and direct comparison with experiments in another report.

In recent years, steady-state magnetic fields have been imposed in melt crystal growth of semiconductor materials to control fluctuations in solute or impurity concentrations caused by chaotic convection in the melt. The action of the field is caused by the Lorentz force induced by the magnetic field when the melt has high electrical conductivity. Increasing the field strength decreases the intensity of cellular convection driven by buoyancy forces. Besides eliminating chaotic and time-periodic convection in large-scale systems sufficient intense magnetic fields decrease the intensity of convection to the point that the axial and lateral variation of the solute concentration in the crystal are affected. The alteration of the laterally-averaged (across the melt/crystal interface) axial concentration of oxygen is one of the primary advantages of using magnetic fields in Czochralski growth of silicon. It is becoming increasingly evident that the lateral uniformity of solute profiles may be adversely influenced by imposed magnetic fields.

Increasing lateral inhomogeneities by decreasing convection mixing is not unexpected. The transition in axial and radial solute segregation from unidirectional crystal growth in the absence of bulk convection to growth with intense laminar mixing is described schematically by the curves shown in Figure 1 in terms of the percentage radial segregation Δ_c, defined as the maximum difference in concentration across the crystal measured as a percentage of the local average, and by the effective segregation coefficient k_{eff} defined as

$$K_{eff} \equiv k \langle c \rangle_I / \langle\langle c \rangle\rangle \qquad (1)$$

where $\langle c \rangle_I$ is the laterally-averaged concentration of a solute at the melt/crystal interface and $\langle\langle c \rangle\rangle$ is the volumetrically-averaged concentration in the melt. In directional solidification, diffusion-controlled growth with a planar melt/crystal interface leads to uniform radial distribution of solutes, i.e. $\Delta_c = 0$. If the melt is sufficiently long that the diffusion layer adjacent to the interface occupies only a small fraction of the total length, k_{eff} is unity in the absence of bulk motion other than the unidirectional growth velocity V_m. The length of the axial concentration gradient can be controlled, since the scale of the diffusion layer is set by the ration D/V_m. Curvature of the melt/crystal interface induces lateral solute variation caused by the focusing of the diffusion field adjacent to the interface.

Weak laminar convection distorts the one-dimensional concentration field and causes the radial and axial segregation indicated on Figure 1. When the mixing of a solute by these flow fields is in-

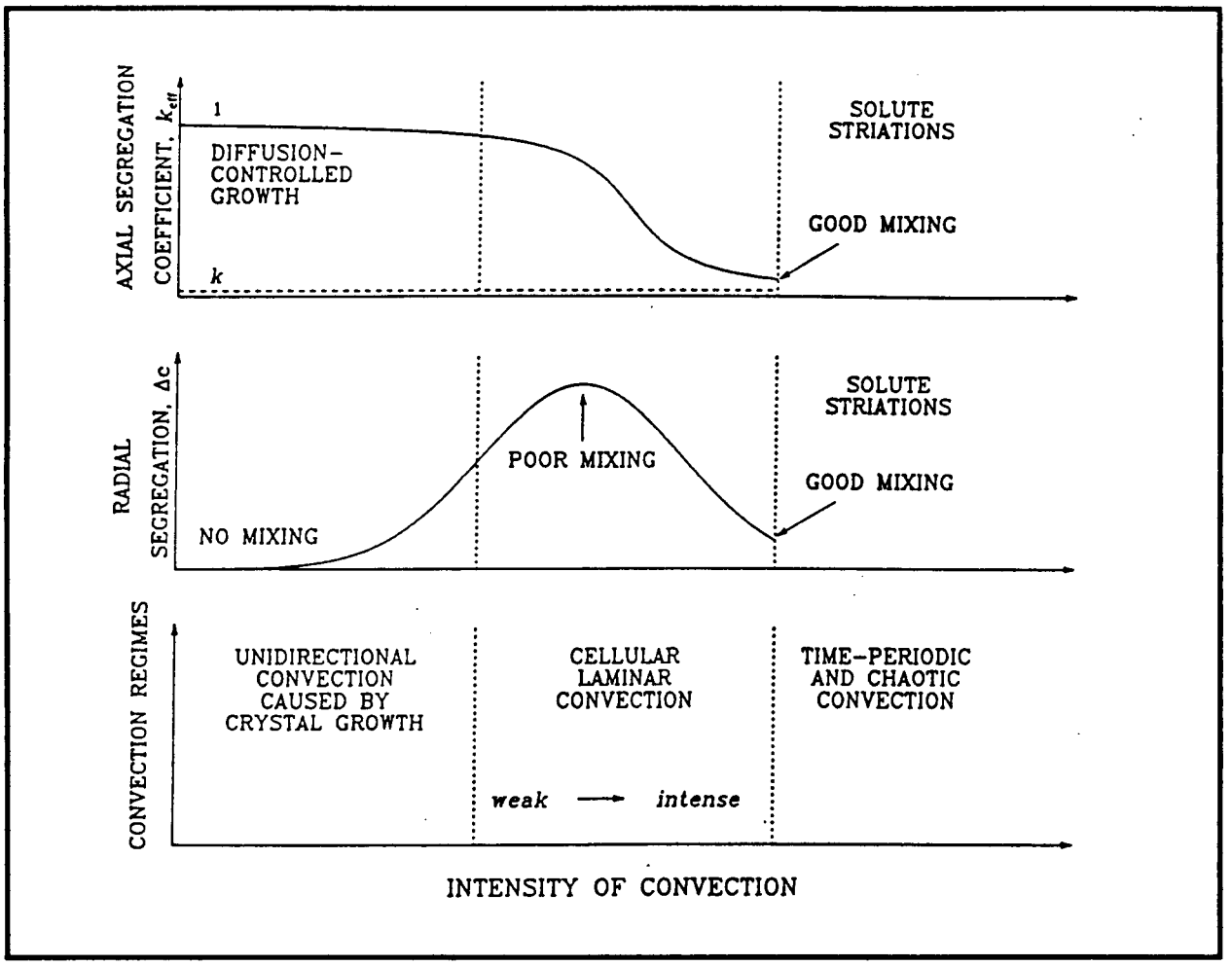

Figure 1. Schematic figure of the effect of flow intensity on the effective segregation coefficient and the percentage radial segregation in a directional solidification system.

complete its concentration field adjacent to the melt/crystal interface can be highly distorted and large amounts of radial segregation are possible, even when the axial composition profile indicate diffusion-controlled growth. Harriott and Brown[3] demonstrated the effect of weak convection caused solely by differential rotation of the feed and crystal rods on radial segregation in small-scale floating zones. This situation exists in well-controlled small-scale crystal growth experiments on earth, in the growth of nondilute binary alloys where the solute field damps convection, in microgravity experiments in which convection has not been stopped entirely, and in experiments with strong magnetic fields.

Solute boundary layers form adjacent to the melt/crystal interface when laminar convection leads to intense mixing. Then the radial segregation of solute decreases and the composition of the melt approaches a new bulk value elevated (assuming $k < 1$) by the mixing of the solute rejected at the interface. In the limit of very thin solute layers k_{eff} approaches k and the solute concentration increases steadily along the length of the growing crystal. Strong laminar convection is rarely found in the low Prandtl number melts of semiconductor materials. Instead time-periodic and chaotic transients in the melt lead to thermal transients near the interface and induce melting and accelerated crystal growth on the time scale for the fluctuation.

The purpose of our work has been to present detailed calculations of the action of a magnetic field on convection, segregation, and heat transfer in a realistic models for the vertical Bridgman

crystal growth system and to quantify the intensity of the field that is necessary to achieve diffusion-controlled, unidirectional solidification in such systems. We have performed calculations for the furnace and ampoule designs for small-scale experiments used in the experimental studies of C.A. Wang (Ph.D. Thesis, MIT, 1984) and Rouzaud et al. (*J. Crystal Growth* 69, p. 149, 1985). The furnace of Wang is a classical Bridgman-Stockbarger system with isothermal hot and cold zones separated by an insulated region designed to create a constant axial temperature gradient in the melt and crystal adjacent to the solidification interface. The furnace of Rouzaud et al. uses a tapered heating element to establish a nearly linear temperature profile over a length of ampoule approximately 30 times the radius of the furnace. The furnaces in both systems are designed so that the crystal growth rate is equal to the ampoule displacement rate after an initial transient caused by the onset of ampoule motion.

Detailed calculations of the temperature fields, melt flow, and axial and radial segregation patterns for these two furnaces were determined for growth of dilute gallium in germanium in both systems without the presence of the magnetic field.[13] Both systems exhibited the transition from diffusion-controlled solute transport to laminar mixing with increasing thermal Rayleigh number. For the conditions of an earthbound experiment, the convection was intense, radial segregation was minimal, and the effective segregation coefficient approached the value of the equilibrium segregation coefficient. In this paper we quantify the levels of imposed magnetic fields necessary to damp this convection to the extent that low radial segregation without axial segregation (k_{eff} - 1) is obtained.

The calculation are based on the finite-element Newton method[14, 13] for the solution of conservation equations and boundary conditions associated with the velocity, pressure, and solute fields in the melt, the temperature in melt, crystal and ampoule, and the shape of the melt/crystal interface. The extension of the method to accommodate the vertical magnetic field is trivial and has been previously described.[17] The abstract of the paper describing the method[17] follows:

> Effect of Vertical Magnetic Field on Convection and Segregation in Vertical Bridgman Crystal Growth, D.H. Kim, P.M. Adornato, and R.A. Brown, *J. Crystal Growth*, (submitted, 1987).
>
> The Petrov-Galerkin/finite-element analysis of vertical Bridgman growth for dilute and nondilute alloys presented before (*J. Crystal Growth* 80 (1986) 155) is extended to include the effect of a vertically-aligned magnetic field in the limit of zero magnetic Reynolds number. Calculations are presented fro growth of a dilute gallium-germanium alloy in a vertically stabilized Bridgman-Stockbarger system and in a furnace with a uniform temperature gradient imposed along the ampoule. Steady cellular convection driven by radial temperature gradients causes good axial and radial mixing in both systems without a magnetic field. A weak magnetic field decreases the intensity of convection and the effectiveness of solute mixing. The radial nonuniformity is greatest for an intermediate field strength. Stronger fields suppress flow recirculation completely and lead to uniform solute segregation across the crystal and to diffusion-controlled axial segregation.

Contours of the temperature, stream function (velocity) and concentration fields are shown in Figure 2 for the thermal Rayleigh number $Ra_t = 1x10^7$ without the magnetic field, i.e. the Hartmann number is Ha = 0. The radial temperature gradients are caused primarily by the differences in the thermal conductivities of melt, crystal and ampoule material and are largest adjacent near the convex melt/crystal interface. The temperature field and interface shape are essentially unaffected by the flow.

The two flow cells are driven by different sets of radial temperature gradients along the ampoule caused by interactions between the furnace and the ampoule. The differences between the thermal conductivities of the melt (k_m = 0.39 W/K cm), the crystal (k_s = 0.17 W/K cm) and the ampoule (k_a =

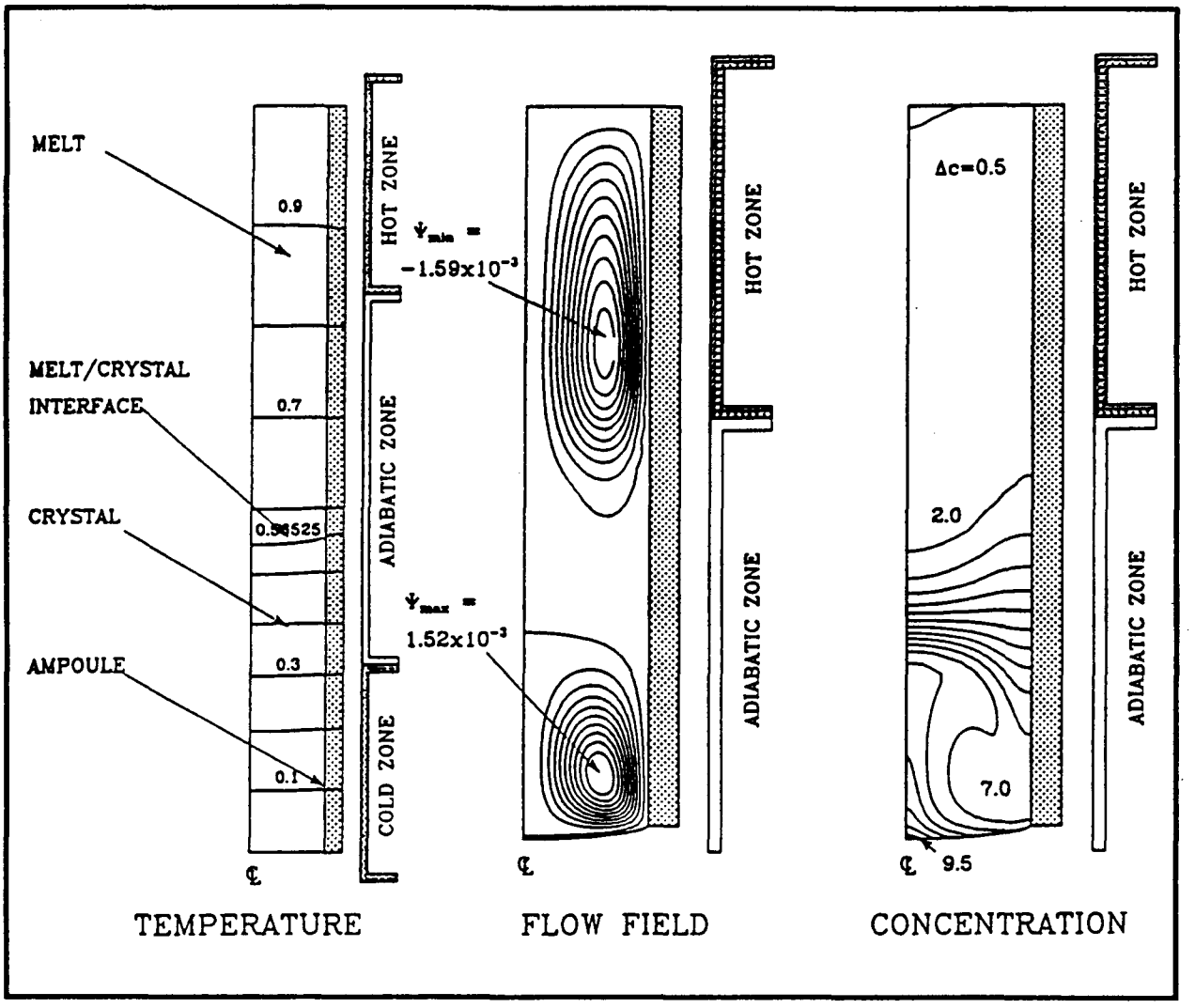

Figure 2. Contours of temperature, stream function, and concentration for growth in the vertical Bridgman furnace with V_g = 4 μm/sec and Ra_t = $1x10^7$. Streamlines are spaced at equal intervals between the maximum (or minimum) values for the cells and zero.

0.26 W/K cm) cause the melt/crystal interface to be convex with respect to the melt and results in the temperature decreasing radially adjacent to this phase boundary. These gradients drive a flow that is up along the axis of the ampoule and down along the wall. Because of the slender shape of the melt, this flow is confined to a portion of the ampoule bottom that is on the order of the ampoule radius.

The mismatch in thermal boundary conditions between the adiabatic and hot zones of the furnace causes a second set of radial gradients with the hottest temperature located at the ampoule wall. The upper flow cell is driven by this part of the temperature field and moves upward at the wall and down along the centerline. The spacing between the two flow cells is controlled by the length of the adiabatic zone.

The gallium concentration field in Figure 2 shows the effects of the mixing caused by both the top and bottom flow cells. The radially uniform and exponentially decreasing concentration field expected without bulk convection is distorted in parts of the melt where either cell is strong. The concentration above the top of the adiabatic zone is essentially uniform because of the upper cell and because the diffusion layer would not penetrate into this portion of the ampoule, even at $Ra_t = 0$. The concentration field near the melt/crystal interface is deformed by the lower cell and the first

stages of the formation of a region of uniform concentration are evident. Steep axial concentration gradients develop in the region of the ampoule between the two cells.

The temperature field and melt/crystal interface for $Ra_t = 1x10^7$ and Ha = 0 are essentially the same as predicted without convection in the melt ($Ra_t = 0$), mainly because of the low Prandtl number for the melt. Increasing Ha has essentially no effect on these variables.

The effects of the axial magnetic field on the flow field is shown in Figure 3. Very weak fields,

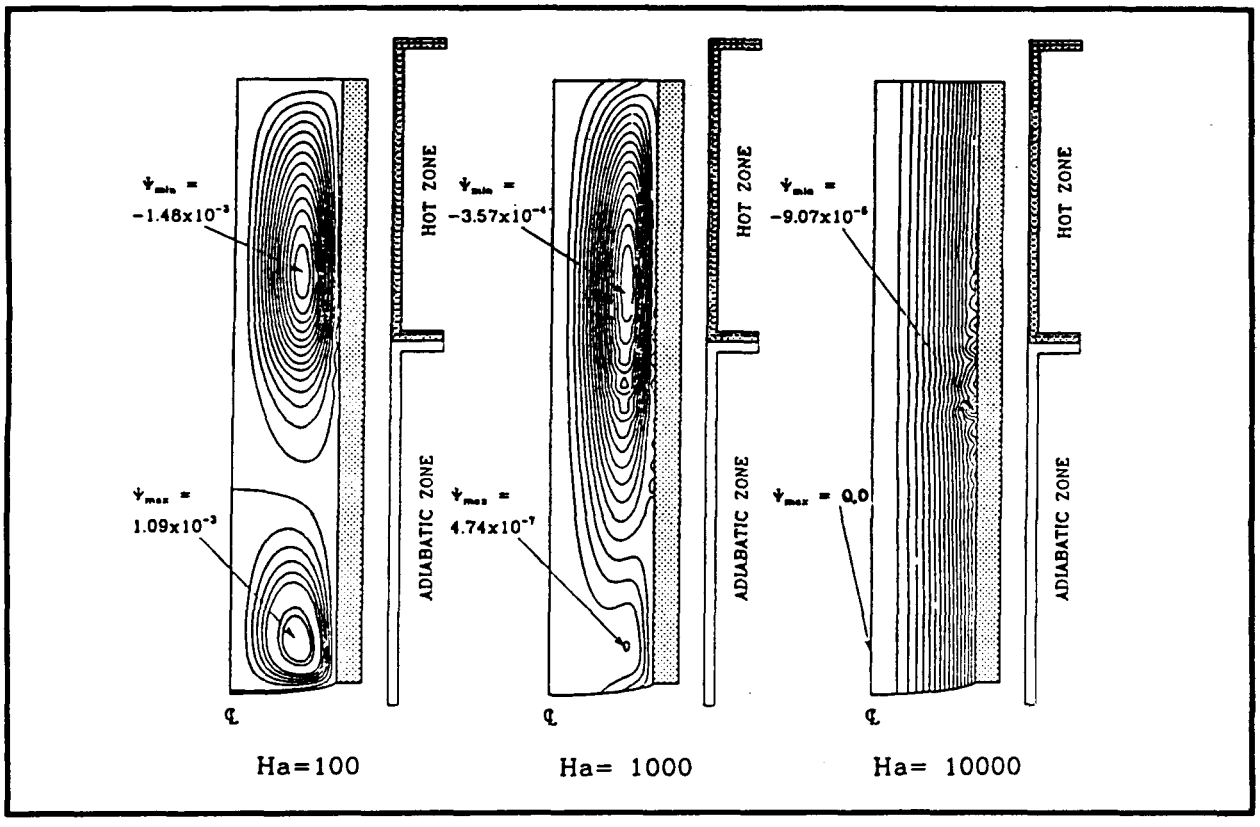

Figure 3. Sample flow fields for growth in the vertical Bridgman furnace with increasing magnetic field strength measured by Ha; $Ra_t = 1 \times 10^7$.

e.g. Ha = 10, decrease the strength of the flow, but leave the flow pattern unchanged. Increasing the field strength causes the flow cell to stretch to fill most of the ampoule, so that more of the flow is aligned with the field and hence unaffected by it. At Ha = $1x10^4$ the cell has disappeared and only the unidirectional motion due to crystal growth remains.

The small value of the solute diffusivity makes the solute concentration field much more sensitive to the level of convection than the temperature field . Solute fields for dilute gallium in germanium are shown in Figure 4, as calculated for the flows shown in Figure 3. The regions of approximately uniform concentration formed by mixing in the two flow cells are still apparent for Ha = 100. The disappearance of the lower flow cell with increasing Ha leads to the reformation of the exponential diffusion layer adjacent to the interface for Ha - $1x10^3$ with weak convective mixing caused. only by the upper flow cell.

The percentage radial segregation Δc is plotted in Figure 5 as a function of Ra_t and Ha for V_g = 4 μm/s. The maximum in Δc occurs for approximately $Ra_t \approx 1x10^6$. The value of Ra_t for the maximum radial segregation increases as the intensity of the field is increased. For Ha > $\geq 1x10^3$ Δc is caused

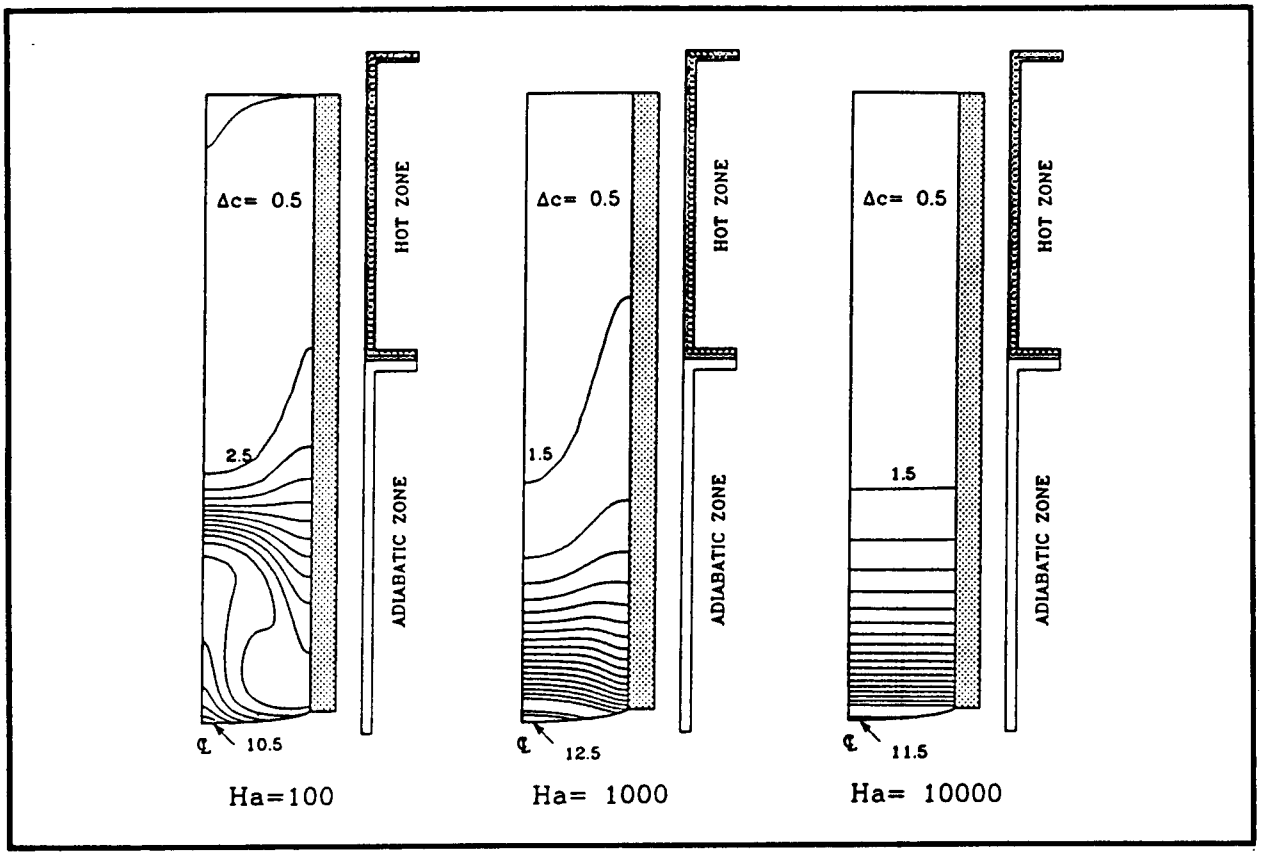

Figure 4. Sample gallium concentration fields for growth of GaGe in vertical Bridgman system with V_g = 4μm/sec as a function of Ha; $Ra_t = 1x10^7$.

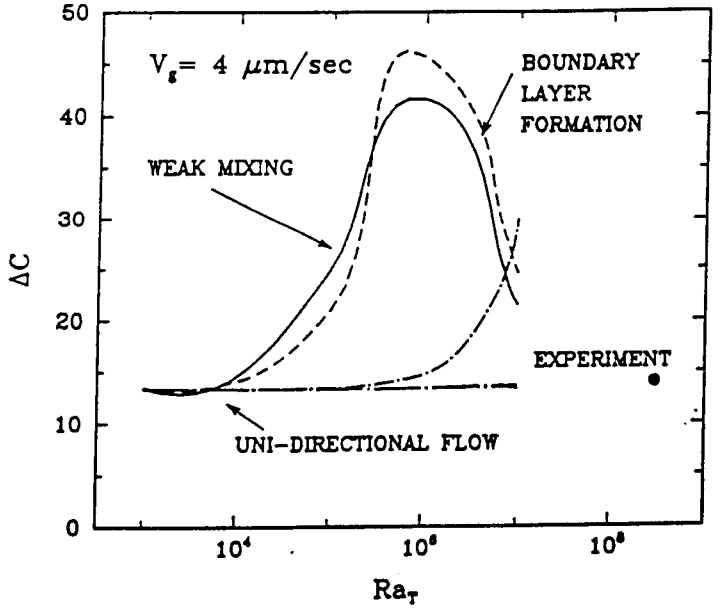

Figure 5. Percentage radial segregation as a function of thermal Rayleigh number and Hartmann number for growth of GaGe in the vertical Bridgman system with Vg = 4 μm/sec. The solid dot corresponds to experimental measurements of Wang.[17]

only the curvature of the melt/solid interface up to $Ra_t = 1x10^7$. calculations at higher values of Ra_t were not possible with the finite element mesh used here because.of the formation of the boundary. The experimental measurement of Wang also is shown; Adornato et al.[13] explained how to extrapolate the numerical calculations to get reasonable agreement with these measurements by using boundary-layer theory for describing the dependence of Δc on Ra_t.

The variation of the axial segregation of solute can be estimated from the calculations with the PSSM by computing the effective segregation coefficient defined by Equation (1). These values are plotted in Figure 6 as a function of Ra_t and Ha. The value of k_{eff} for low convection (Ra_t - 0) is not

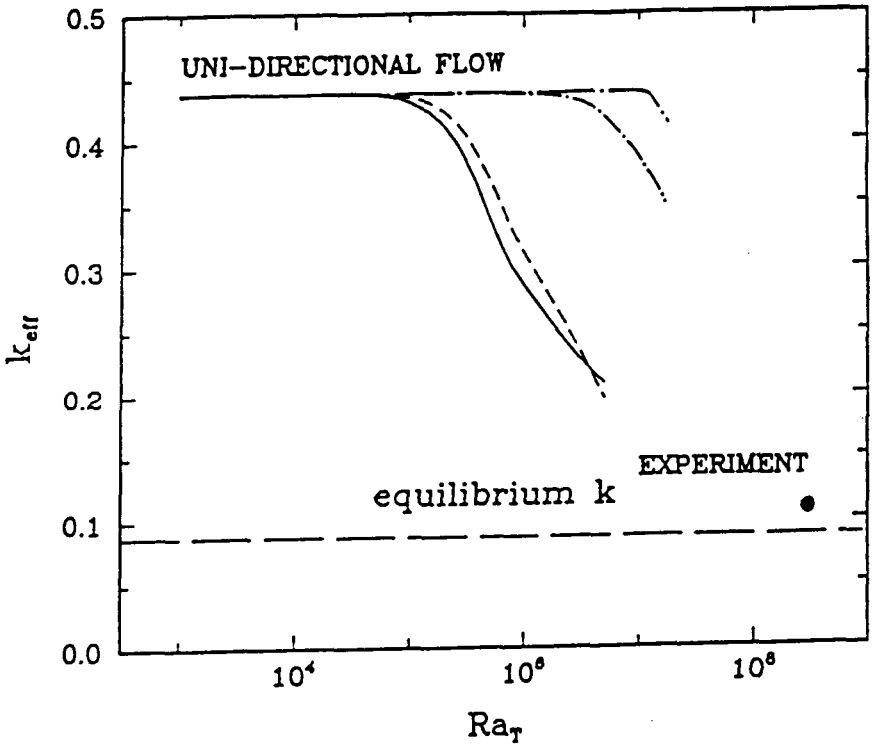

Figure 6. Effective segregation coefficient computed from equation 1 as a function of Ra_t and Ha for growth in vertical Bridgman furnace with V_g = 4 μm/sec. The solid dot correpsonds to the experimental measurement of Wang.

unity because the ampoule is not long enough for the variation in concentration caused by the diffusion layer to be small relative to the portion of the melt which is at the bulk concentration (c = 1). The increased mixing caused by convection and the decrease in k_{eff} towards the equilibrium value (k = 0.087) are obvious. Increasing the magnetic field strength increases the effective segregation coefficient, shifting the critical value of Ra_t for the beginning of the decrease in k_{eff} to higher values. The experimental measurement of Wang without a magnetic field is again shown for reference.

Direct comparison between these calculations and experiments with strong magnetic fields are underway. The experimental data is being supplied by Prof. A.F. Witt through research also funded by NASA.

Microscopic Modelling of Pattern Formation in Two-Dimensional Solidification

Morphological stability theory describes the mechanisms for a smooth solidification front separating a binary melt form its solid to develop undulations that lead to cellular and dendritic

structures on the microscale. Although the onset of morphological pattern formation is well understood from linear stability theory pioneered by Mullins and Sekerka, the transitions to deep cellular and dendritic structures are not. Our theoretical and experimental program is aimed at this goal for two-dimensional, thin-film solidification experiments where quantitative experiments are possible.

We have developed asymptotic and numerical methods aimed specifically at analysis of pattern formation in two-dimensional solidification experiments. The development of these techniques is discussed in a number of our publications[5, 16]. The results from several recent publication are discussed in the following section on the theoretical analysis of two-dimensional solidification. Our research program has expanded from a purely theoretical and computational effort to the development of a precise experimental system for studies of two-dimensional solidification, as analyzed by our calculations. This system was developed during this year of NASA support and is outlined in the section entitled "Experimental System".

Theoretical Analysis of Two-Dimensional Solidification

Analysis in the previous year has focussed on two aspects of microscopic pattern formation in two-dimensional solidification. First, is an explanation for the lack of experimental observation of the spatial wavelength for small-amplitude cells predicted by linear stability theory, as reported by a number of experiments in recent years. The second issue is the transition to deep cellular patterns and the possibility of a mechanism for selection of a specific spatial wavelength from the large range of linearly unstable ones. Each of these issues is discussed in the review paper abstracted below:

> "Numerical Analysis of Cellular Solidification Microstructures," R.A. Brown, N, Ramprasad, M.J. Bennett, *Supercomputers in Chemistry and Chemical Engineering* ACS Symposium, eds. K. Jensen and D. Truhlar (ACS, 1987).
>
> *Large-scale numerical calculations are used to simulate the formation of cellular microstructures during directional solidification of a binary alloy. The analyses are based on finite-element methods developed especially for solving the free- and moving-boundary problems that describe the solute field in melt and solid and the melt/solid interface shape in the Solutal Model of microscopic solidification. Calculations are reported for individual cells that show the transitions from steady-state solidification of shallow cells bear the onset of morphological instability to deep cells separated by narrow grooves as seen in experiments. Simulations with multiple cells show the importance of nonlinear interactions between shapes with resonant spatial structures in determining the time-dependent dynamics of large collections of cells. The results of cellular dynamics calculations fro multiple cells show the possibility of long time-scale time-periodic and quasi-periodic interactions.*

Analysis of nonlinear transitions in shallow and deep, two-dimensional cells are discussed separately below.

Nonlinear transition for shallow cells

The key feature of directional solidification systems which leads to the complex nonlinear interactions seen experimentally is the flatness of the small surface energy associated with the melt/crystal interface. Since the surface energy is the sole effect which stabilizes a planar interface against short wavelength instabilities, the resulting neutral stability curve for the onset of cellular growth is extremely flat. This is seen in Figure 7, for a set of thermophysical properties similar to PbSn, except that the solute diffusivity in melt and solid is taken to be the same. Note that approximately the same value of the growth rate $V_c(\lambda)$ leads to instability for a band of wavelengths which stretches over an order-of-magnitude. This flatness of the neutral stability curve leads to nonlinear interactions between spatial resonant values of the wavelength lower than the critical value predicted by linear

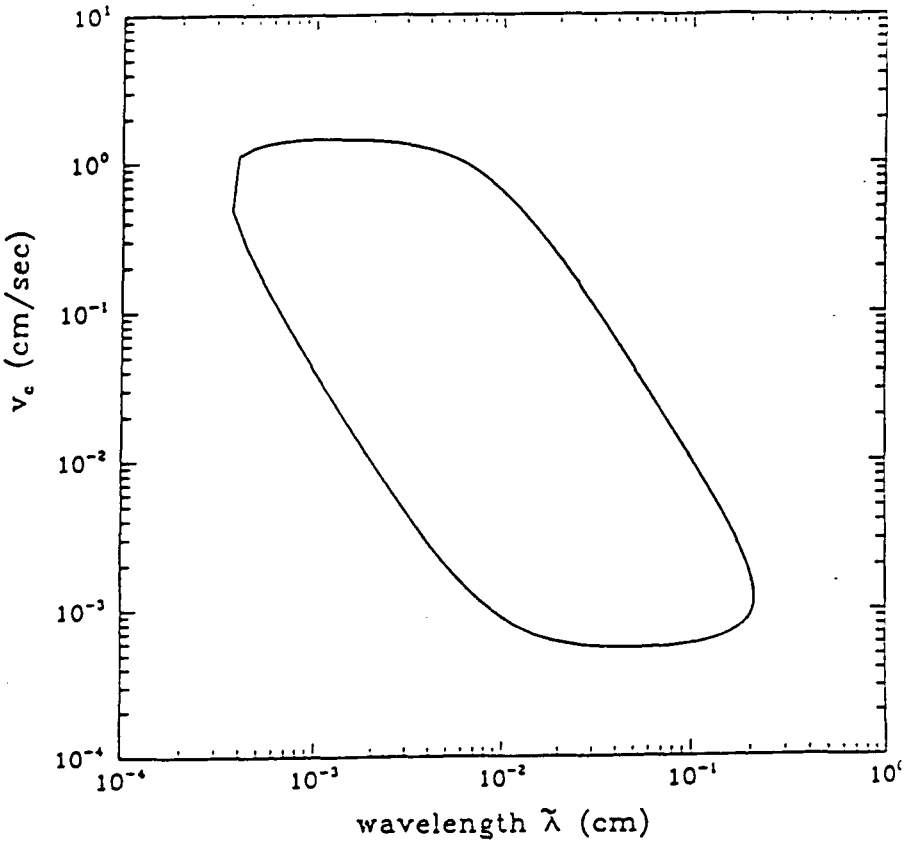

Figure 7. Neutral stability curve predicted from linear analysis for values of the thermophysical properties appropriate for PbSn, buth with equal diffusivities in melt and solid.

theory, as observed in the experiments. The theoretical development of this observation is given in the reference below along with detailed nonlinear calculations:

> "Nonlinear Interactions of Interface Structures of Differing Wavelength in Directional Solidification," M.J. Bennett, R.A. Brown, and L.H. Ungar, Proceedings of the International Symposium on the Physics of Structure Formation (Springer-Verlag, 1987).
>
> **The solution structure of the cellular patterns formed during the directional solidification of a material containing a dilute impurity is studied by numerical analysis of a simple model. Solution families corresponding to cells of different spatial wavelength arise as the growth velocity is increased above the value for the onset of the instability. The resonant interaction between these steady-state shapes leads to both stable and unstable time-periodic oscillations. Only some of the oscillatory interface structures computed have been predicted by normal mode analysis of codimension-two bifurcations. The interactions between cells with different spatial structures limit the range of validity of asymptotic expansions to a velocity range too small to be reliably measured experimentally.**

The nonlinear transitions caused by these codimension-two bifurcations are demonstrated in Figure 8 by calculations of cells with specific wavelengths as a function of the dimensionless growth rate $P \equiv V\lambda/D$, where D is the solute diffusivity. The thermophysical properties for these calucations are the same as used in the calculation of the neutral stability curve, Figure 7; the sample size $\lambda_c = 4.5$ correpsonds to the most unstable wavelength predicted from this figure. Nonlinear cell shapes with

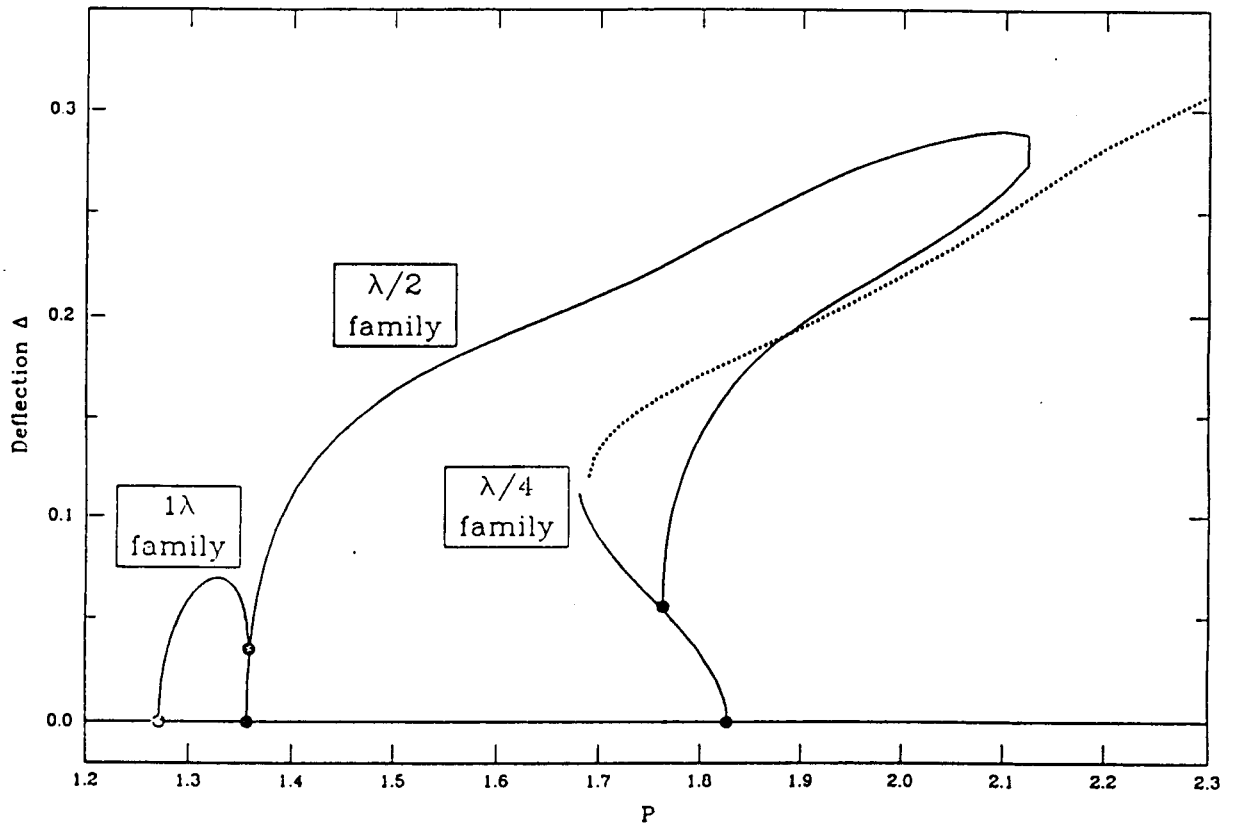

Figure 8. Families of steady-state shapes computed as a function of increasing growth rate P in a $\lambda_c/2$ sample size.

this wavelength evolve from the critical value $P = P_c(\lambda)$ predicted by linear theory. Two secondary bifurcation points are computed for $P < 2P_c(\lambda_c)$ which reduce the wavelength of the computed cell shape to $\lambda_c/4$. The amplitude of the cells is represented by the dimensionless cell depth defined as

$$\Delta \equiv \Delta / \lambda \qquad (2)$$

where Δ is the dimensional value and λ is the dimensional cell wavelength. Representative cell shapes are shown in Fig. 9 to demonstrate the steepening of the cell shape with increasing Peclet number. Calculations with the Monge interface representation were stopped because of the possibility that the interface would become reentrant, signifying that the solid melts and then resolidifies in the groove.

Figure 9 shows interface shapes computed using this representation with fixed wavelength $\lambda = 1$ and increasing P. The long cells have a distinct three-region structure with a rounded tip, a long sidewall and a small bottom. Increasing he Peclet number lengthens the sidewall relative to the other regions, and suggests an asymptotic structure.

We feel that the dynamics of wavelength selection for shallow cellular interface structures is best described as a statistical average of the dynamical behavior of a collection of cells over a long time. We are pursuing this approach through cellular dynamics calculations.

Wavelength Selection in Large-Amplitude Cells with Finite Depth

The calculations discussed above lead to the conclusion that no mechanism exists for selection of a specific spatial wavelength for shallow cells near the onset of pattern formation. To test for the

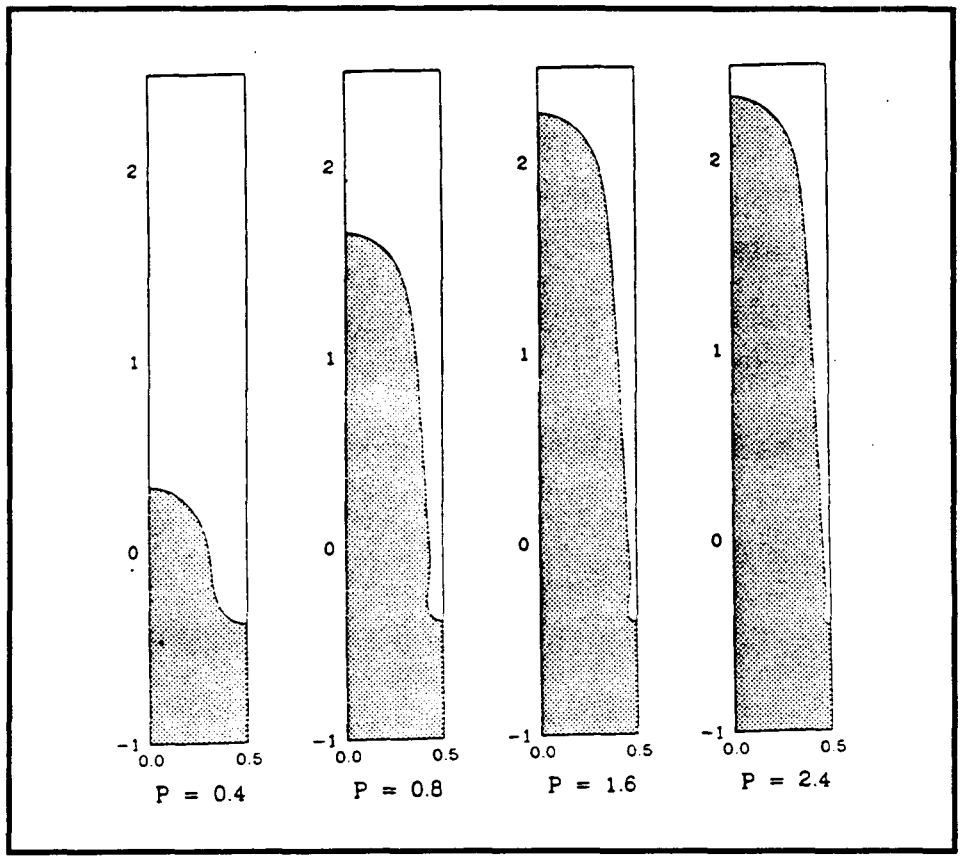

Figure 9. Sample interface shapes for increasing P and $\lambda = 1.0$ as computed with the method described by Ungar and Brown.[6]

existence of a mechanism for wavelength selection calculations for relatively deep cell. The abstract of the paper based on these calculations is given below.

> "Wavelength Dependence of Cells of Finite Depth in Directional Solidification," N. Ramprasad, M.J. Bennett, and R.A. Brown, Phys. Rev. A. (submitted, 1987).
>
> Finite element calculations are presented for individual shapes in a spatially period pattern of two-dimensional cellular interfaces that occur during the directional solidification of a binary alloy. The transition from shallow sinusoidal cellular shapes to cells separated by deep grooves is computed as a function of the spatial wavelength of the pattern as the growth rate is increased. The flatness of the neutral stability curve is responsible for secondary bifurcations that result from nearby codimension-two critical points. Tip splitting of the cells results and the apparent wavelength decreases by multiples of two from the value predicted by linear stability theory. Deep cells with rounded tips, linear sidewalls and pendent shaped bottoms are computed for a range of spatial wavelengths and growth rates, so that no mechanism for singling out discrete wavelengths is apparent. A wavelength corresponding to the cell with maximum depth is predicted as a function of the growth rate.

Figure 10 shows these calculations. The velocity is constant along each curve and is reported as a multiple of the critical value for the most dangerous wavelength $V_c(\lambda_c)$. Along each curve G and P decrease and Γ increases as λ is lowered. An important feature is that for each growth rate there is a deepest cell and this cell occurs for a decreasing value of the wavelength with increasing growth rate. For growth rates as low at (1.9) $V_c(\lambda_c)$ this maximum occurs at wavelengths less than $\lambda = 1$, compared to $\lambda_c = 4.5$. This is not unexpected, because the wavelength splitting mechanisms demonstrated in

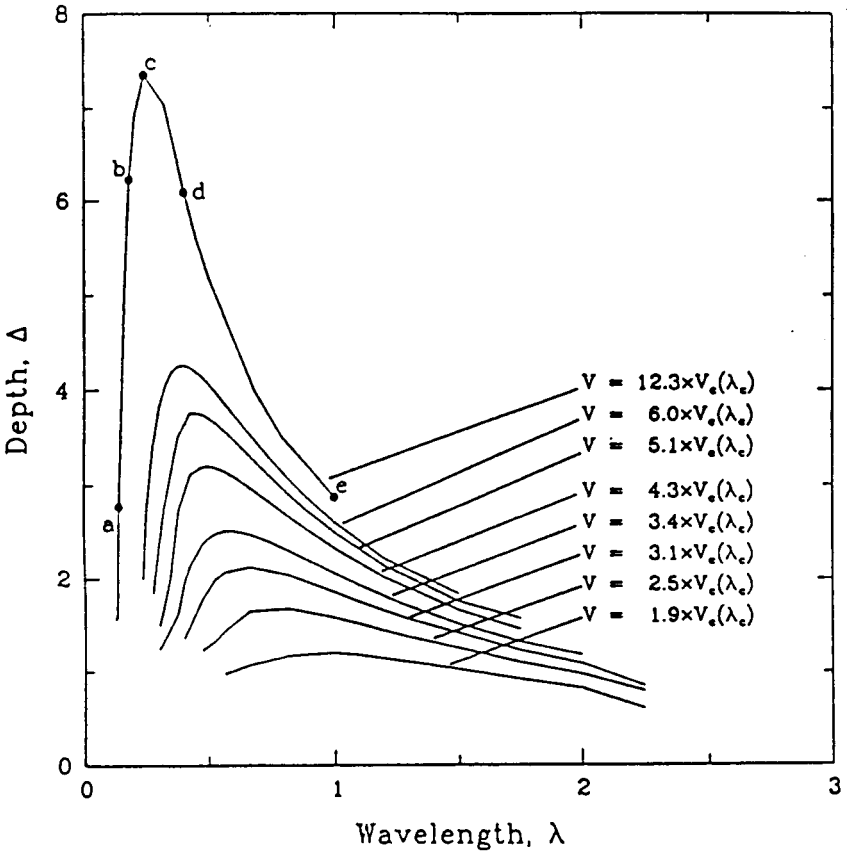

Figure 10. Dependence of cell depth on wavelength for specific values of growth rate P and other parameters held fixed.

Figure 10, indicate rapid transitions to shorter wavelengths. Deep cells ($\Delta > 2$) are computed within an increasingly narrower band of spatial wavelengths as the growth rate increases. This is an important observation because it gives evidence that some wavelength selection toward smaller values of λ does occur when the transitions from shallow cells to ones separated by deep grooves is considered.[19]

Sample cell shapes for varying wavelengths along the curves with the highest growth rate are shown in Figure 11 rescaled so the lateral dimension of each cell varies between zero and one. The top and bottom of the cell shape for the shortest wavelength (11a) are extremely rounded, showing the dominant influence of surface energy in these regions. Calculations cannot be continued to lower values of λ using the mixed cylindrical/cartesian representation.[19] As the cell lengthens with increasing λ, a long sidewall or groove forms that separates the tip from the bottom. The interface shape and the axial variation of the concentration field are linear along the sidewall, showing that the contributions from the temperature field and the liquidus curve dominate the Gibbs/Thomson equation and that surface energy contributions are unimportant in this region. The cell bottoms are self-similar with increasing λ, but decrease in size relative to λ, because the capillary constant decreases proportional to λ.

The calculations for a single deep cell, but with a bottom suggests that adequate modelling of the dynamics of real cells probably must account for more detail of the cellular structure than is currently being considered in studies of idealized problems. Because of the finite length of these structures, the small surface energy seems to be controlling the length of the cell and selection of the wavelength through interactions that involve the matching of regions of the shape, like the tip and the sidewall

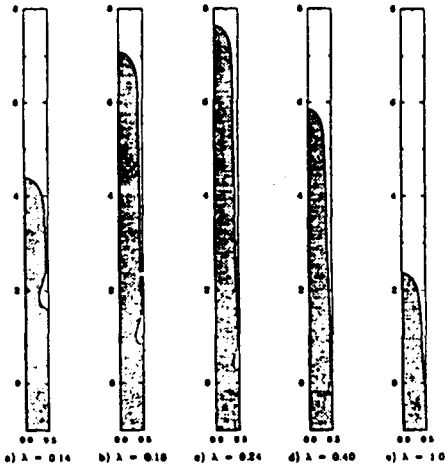

Figure 11. Cell shapes for representative calculations from Figure 10 and the highest growth rate. The letters for these shapes correpsond to the points shown on Figure 10. the wavelengths have been normalized so that the aspect ratio of the cells, measured as Δ, can be compared directly.

where it is relatively unimportant with the highly curved cell bottom. There is some hope that this structure can be captured by asymptotic analysis for simple solidification models; large-scale calculations are playing an important role in developing such a theory. A similar relationship may exist between the shapes of the tip and the sidebranching along a freely growing dendrite in directional solidification.

Experimental System

We have developed a quantitative thin-film solidification experimental system using the succinonitrile-acetone system, video imaging, digitization, and statistical data analysis to provide the framework for direct comparison with the calculations described above. The experiments differ from those performed previously in several important ways which will remove the ambiguities from the measurements:

a. Care is taken to control the pull rate within 1% of the critical value.

b. A long sample is used to insure that transients have decayed and that there is ample time for statistically meaningful data acquisition.

c. The video imaging system will lead to quantitative date on both the local cell shape and statistics on the cell front.

A. Solidification System

The solidification system designed for this experiment consists of long glass plates held in place by a metal support, as shown in Figure 12. The alloy is loaded into the sample through fill ports at either end. The sample is attached to a translating stage (Control Technics Corporation) which is surrounded by a thermal environment constructed from hot and cold water baths separated by a nearly adiabatic region. The sample can be translated through the temperature field at rates between 1 and 100 μm/s at an accuracy of ± 0.1 μm/s, as set by the accuracy of the translation device. Although this accuracy is far better than previous experiments, it is not sufficient to support growth rates as low as

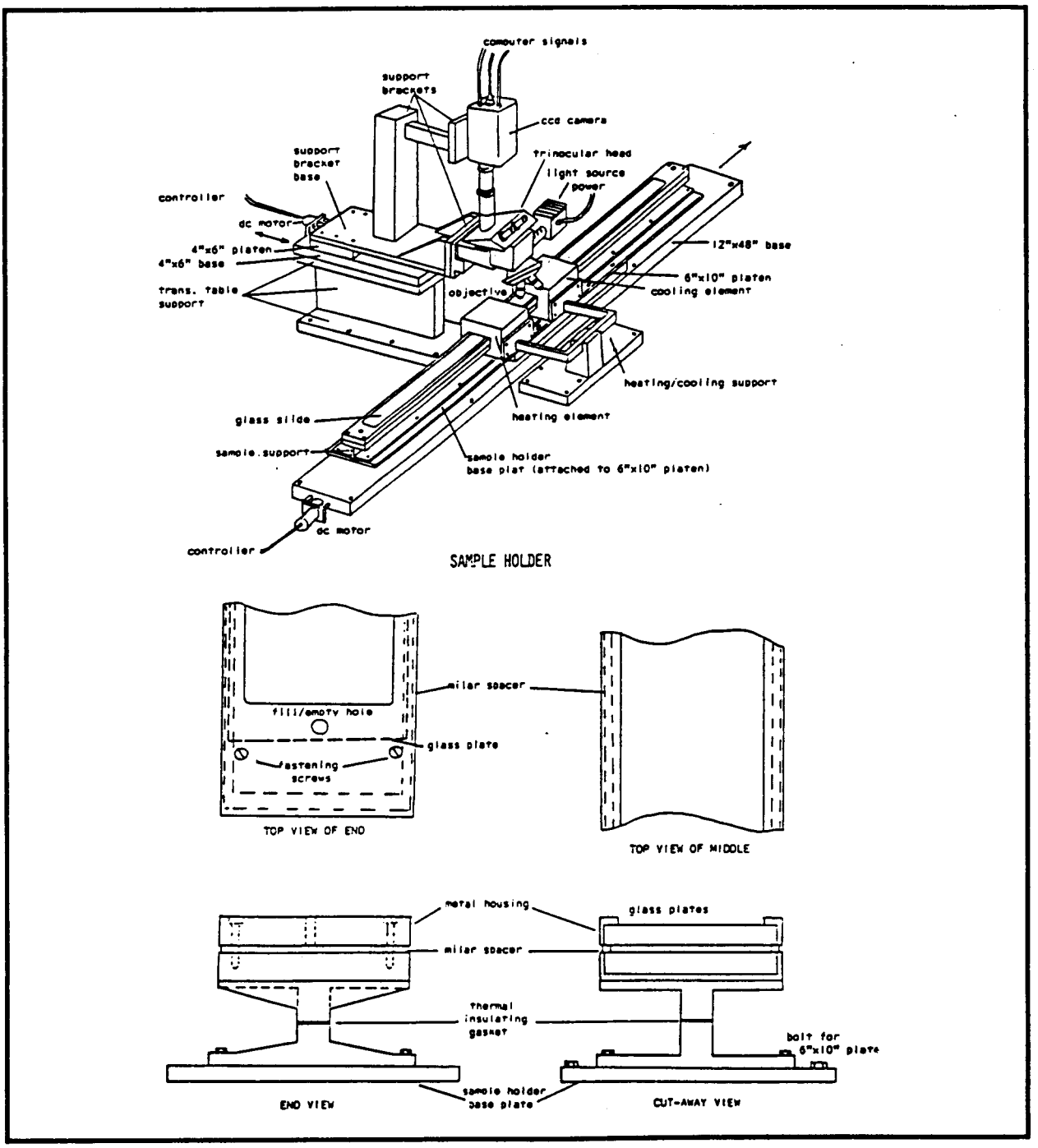

Figure 12. Schematic of proposed thin-film solidification system: (a) total system and (b) sample holder.

1.0 μm/s, as have been use previously where significant nonlinear interactions along the front are predicted to occur P less than 5% beyond P_c. We plan to use lower concentrations and higher growth rates so that the growth velocity can be control accurately enough to distinguish the nonlinear transitions.

The sample optical microscope is mounted to the lateral component of the translation stage so that the entire solidification front can be traversed. The translation system and furnace have been sized so that a sample 100 cm long can be accommodated. This length is necessary for comparison

with the long time scale evolution of shallow and deep cells predicted by the dynamical calculations to date and to gather time-dependent statistics for making quantitative measurements of possible chaotic interactions.

B. Alloys

Initial experiments will be conducted using the succinonitrile-acetone alloy. We have chosen this system because its thermophysical properties are extremely well characterized an because the alloy is chemically stable for long time periods. We plan to purchase the succinonitrile from Prof. Glicksman at RPI. Marginal stability curves for this alloy are shown in Figure 13 as a function of the

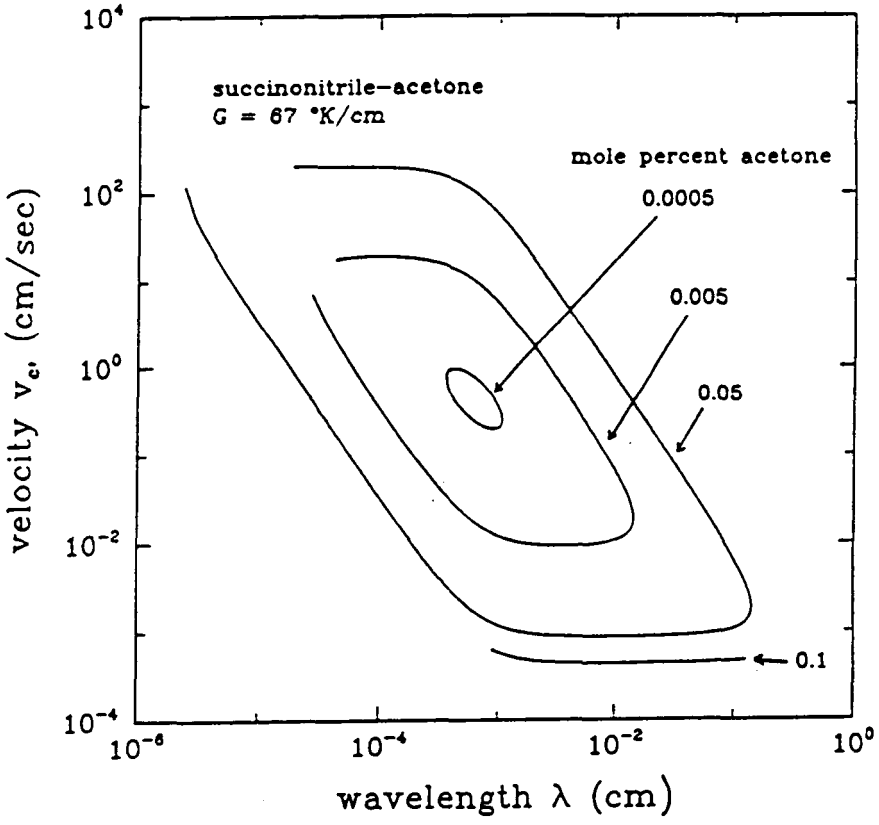

Figure 13. Neutral stability curves for succinonitrile-acetone system as a function of acetone concentration for fixed temperature gradient of 67°/cm.

acetone concentration. By decreasing the acetone concentration; to 0.01-0.05 mole %, the growth rate at the onset of instability can be increased to over 10 μm/s and the range of unstable wavelengths can be decreased significantly; compare the lateral extent of the curves for decreasing concentration. We expect the number of interacting wavelengths to decrease with decreasing concentration, so that steady-state forms are easier to obtain.

The need purity of succinonitrile is attainable by a combination of vacuum distillation and zone refining, as outline by Huang and Glicksman (Acta Metall. 29, p. 701, 1981). Purities of up to 99.9999% have been reported by these authors. Introduction of impurities during the loading of the sample will be avoided by hermetically joining the purification apparatus with the sample holder. The acetone will be added during the filling of the sample.

C. Data Acquisition and Analysis

A CCD camera fitted to a microscope with a 5-50x objectives is used to gather video images of the cellular interface, with approximately ten cells being viewed. Video images of the cellular front from the CCD camera are to be simultaneously recorder with a video recorder and processed through a Recognition Technologies Inc. (RTI) image processing system. This system will be configured to perform edge enhancement and recognition of up to 30 gray scale images (512x512 pixels) per second using software provided with the system. Because we expect the microstructure to evolve slowly in time (the growth of one wavelength of interface will take about 60 seconds), the RTI system should supply amble computational power for simultaneous analysis of the cellular structure within four laterally adjacent view ports for the objective, as controlled by the lateral translation of the stage, so that the dynamic interactions of approximately forty cells can be monitored.

Data in the form of the spatial locations of points along the interface will be passed into an IBM AT computer for storage and post-processing. The computer also controls the growth rate of the sample and the lateral location of the microscope objective. The data will be analyzed in several ways:

1. The melt/solid interface will be reconstructed and compared to the stored video images. This numerical form of the experimental data can be used for comparison with the asymptotic and numerical analyses described above.

2. Statistical information about the time evolution of the microstructure will be develop[ed by performing Fourier analysis on the interface shaped and computing correlation functions as a function of time. Software is available from RTI for these purposes. Simple quantities like the spatially-average wavelength as a function of time will be available as a result of this analysis. The correlation functions will give a direct indication of whether the interpretation of this average as a unique wavelength for the microstructure is meaningful.

Analysis of Small-Scale Floating Zone Systems

The reduced gravity environment of an experiment in space helps overcome considerable limitations to the floating zone process for growth of single crystals that exist on earth and make the study of this system of considerable importance to NASA's microgravity program. We have developed a detailed thermal-capillary model of the transport phenomena and interfacial phenomena important in small-scale floating zone systems. A schematic of this system is shown in Figure 14. Here a cylindrical rod of polycrystalline material is melted and resolidified into a single crystal by using a short circumferential radiative heater that translates slowly along the axis of the rod. The molten zone forms between the crystal and the feed rods and is held in place by surface tension. Its size is governed by heat transfer and limited by instabilities that have been assumed to originate at the meniscus. The radius of the rod is limited by the interaction of gravity with the shape of the meniscus and with heat transfer. We have developed a thermal-capillary model that accounts for these couplings and so can predicted operating conditions for small-scale floating zones. The model has been developed in two steps Figure 14 shows a schematic of a small-scale floating zone heater by a source with a Gaussian distribution.

First, a conduction-dominated model was described[18] that included the effects of the couplings between heat transfer and zone shape, but neglected convection in the so that the major heat transfer mechanisms modelled were conduction in each phase and radiation between melt and solid and the surroundings. Numerical solution of the free-boundary problem which describes the temperature field in each phase, the shapes of the two melt/solid interfaces and the meniscus has been by a

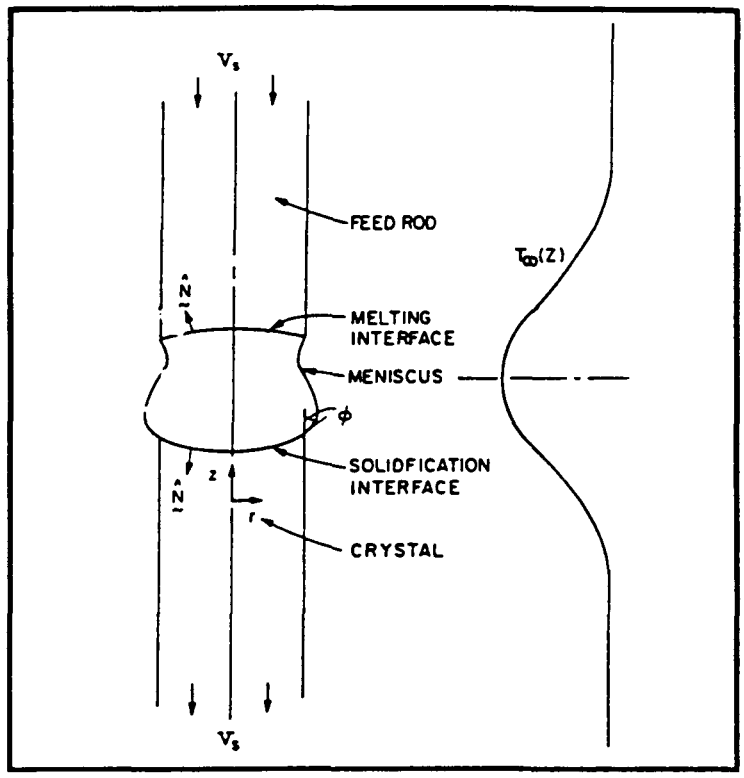

Figure 14. Schematic of small-scale floating zone system.

Galerkin finite-element method combined with Newton iteration which simultaneously compute corrections for all these variables. The development of this model, the numerical method and predictions for small-scale.silicon zones were described in a previous publication.[12]

Research in the last year has focussed on extending the analysis to include a description of fluid flow in the melt driven by buoyancy forces, surface tension gradients and rotation of the feed and crystal rods. The step is necessary to allow prediction of operating states for larger scale zones and materials with high Prandtl numbers, e.g. oxides, where convection in the melt is an important mechanism for heat transfer.

Incorporation of the fluid mechanics of the melt into the analysis has been straightforward, but tedious task. A mixed finite-element approximation to the velocity and pressure fields in the melt have been added along with Galerkin approximations to the momentum equation with the Boussinesq approximation and to the condition for incompressibility. These additional equation have been incorporated directly into the Newton iteration used in the conduction-dominated thermal-capillary model. The size of the matrix problem that must be solved at every Newton iteration has increased enormously; 2000 variables are typical for the conduction-dominated model, whereas 25,000 are needed for accurate approximations that include realistic flow in the melt. To do this has required the development of an out-of-core equation solver especially for the structures matrices that arise in application of Newton's method to free-boundary problems.

The testing of the finite-element code for solution of the thermal-capillary model with convection is just complete and simulations of specific growth systems, e.g. silicon, are underway. These results, as well as the development of the finite-element technique, will be reported later. This report only includes one example of calculations with this program to demonstrate the intensity of convection in even small-scale floating zones.

The flow fields appropriate for surface-tension driven flows in a self-consistent model of a 1 cm. radius silicon floating zone is shown in Figure 15 as a function of the Marangoni number, which is de-

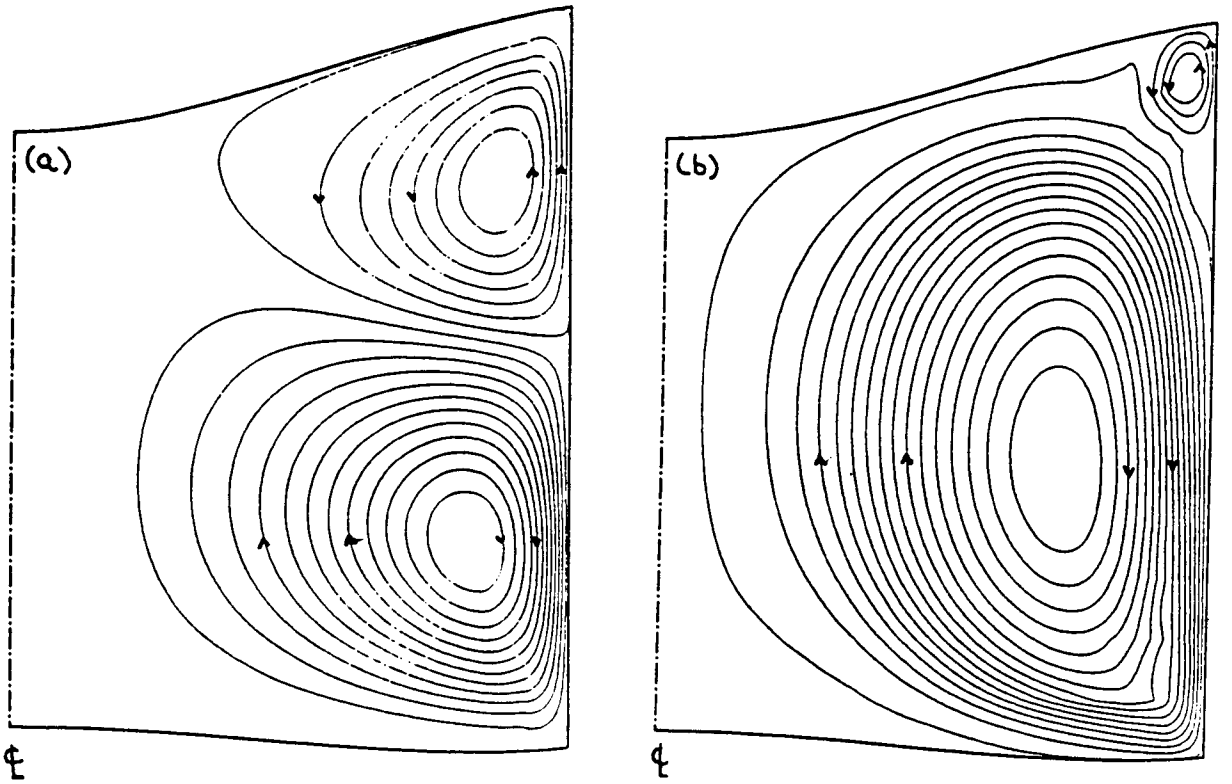

Figure 15. Stream function representation of flow patterns driven by surface-tension gradients for a small-scale silicon floating zone: (a) Ma - 100 and (b) Ma - $1x10^4$.

fined here as $Ma \equiv (\partial\sigma/\partial T)T_m R/\alpha\mu$; values close to $1x10^6$ are appropriate for silicon. The shape of the meniscus has been idealized in these calculations as a cylinder by setting the gravitational acceleration to zero and the wetting angle between the melt and crystal to 90°. The stream function contours plotted in Figure 15 show the importance of momentum convection in determining the flow pattern. The two cell flow pattern predicted by asymptotic analysis for a zone with heat supplied by a Gaussian source and for low Ma is only correct in that parameter region. Inertia causes the lower cell to compress the upper one against the melting feed rod giving the distorted patterns seen for higher Ma.

Publications and Presentations of Research Supported by Grant NSG-7656 (Since 1984)

Publications

1. G.M. Harriott and R.A. Brown, "Flow in a differentially rotated cylindrical drop at moderate Reynolds number," *J. Fluid Mech.* 144 (1984): 403-418.

2. L.H. Ungar and R.A. Brown, "Cellular interface morphologies in directional solidification. 2. The effect of grain boundaries," *Phys. Rev.* B 30 (1984): 3993-3999.

3. G.M. Harriott and R.A. Brown, "Flow structure and radial dopant segregation in small-scale floating zones," *J. Crystal Growth* 69 (1984): 589-604.

4. R.A. Brown, L.H. Ungar, and P.A.Adornato, "Convection, Segregation and interface morphology in directional solidification," *Proceedings of the Aachen Workshop on Solidification and Microgravity*, ed. P. Sahm (Aachen, West Germany, 1984), pp. 127-157.

5. R.A. Brown, "Status of modeling of convection, segregation, and interface morphology in melt growth of semiconductor materials," *Proceedings of Workshop on Microgravity Science and Applications* (National Research Council, December 1984).

6. E.D. Bourret, J.J. Derby and R.A. Brown, "One-dimensional modelling of transients in directional solidification of nondilute binary alloys," *J. Crystal Growth* 71 (1985): 587-596.

7. L.H. Ungar, M.B. Bennett, and R.A. Brown,, "Cellular interface morphologies in directional solidification. 3. The effect of coupled heat transfer," *Phys. Rev.* B 31 (1985): 5923-5930.

8. L.H. Ungar and R.A. Brown, "Cellular interface morphologies in directional solidification. 4. The formation of deep cells," *Phys. Rev.* B 31(1985): 5931-5940

9. R.A. Brown, "Physical process modelling: large-scale integration for complex physical system," *Proceedings of the NSF Workshop on Large-Scale Scientific Computing in the Chemical Process Industries* (December 1985).

10. R.A. Brown, "Convection and species transport," *Materials Sciences in Space*, eds. B. Feuerbacher, H. Hamacher, and R.J. Naumann (Berlin:Springer-Verlag, 1986), pp. 55-94.

11. R.A. Brown, "Modelling of transport processes in melt crystal growth," *Proceedings of the First International Conference on the Processing of Electronic Materials*, ed. C. Law (New York:Springer-Verlag, 1986, in press).

12. J.L. Duranceau and R.A. Brown, " A thermal-capillary model for the floating zone crystal growth process," *J. Crystal Growth* 75 (1986): 367-389.

13. P.M. Adornato and R.A. Brown, "The effect of ampoule on convection and segregation during vertical Bridgman growth of dilute and nondilute binary alloys," *J. Crystal Growth* 80 (1987): 155-190.

14. P.M. Adornato and R.A. Brown, "Petrov-Galerkin methods for natural convection in directional solidification of binary alloys," *Int'l. J. Numer. Meths Fluids* 7 (1987): xxx-xxx.

15. P. Sackinger, R.A. Brown, and G.B. McFadden, "Eigenfunction expansions for determining structure of natural convection in a vertical cylinder heated from below," J. Fluid Mech. (1987, submitted).

16. L.H. Ungar, N. Ramprasad, and R.A. Brown, "Finite element methods for unsteady solidification problems arising in the prediction of morphological structure," *J. Sci. Comput.* (1987, submitted).

17. D.-H. Kim, P.M. Adornato, and R.A. Brown, "Effect of vertical magnetic field on convection and segregation in vertical Bridgman crystal growth," *J. Crystal Growth* (1987, submitted).

18. F.T. Geyling, M.J. Crochet, and R.A. Brown, "Computer simulation of bulk crystal growth; a link between basic research and product engineering," *Science* (1987, in preparation).

19. N. Ramprasad, M.J. Bennett, and R.A. Brown, "Wavelength dependence of cellular forms for directional solidification cells with finite depth," *Physical Review B* (1987, submitted).

20. R.A.Brown, "Transport processes in melt crystal growth," *Chemical Engineering in Microelectronics*, ACS Volume, eds. K.F. Jensen and D. Hess (1987, in press).

21. R.A. Brown, "Convection and solidification in melt crystal growth," *Advanced Crystal Growth*, ed. P. Dryburgh (1987, in press).

22. L.G. Leal and R.A. Brown, "Fluid Mechanics of Microstructure Fluids," Report to NSF on Fluid Mechanics (1987, in press).

23. R.A. Brown, "Numerical analysis of solidification microstructure," *Supercomputer Research in Chemistry and Chemical Engineering*, ed. D.G. Truhlar and K.F. Jensen, ACS Symposium Series (1987, in press).

24. R.A. Brown, L.J. Atherton, J.J. Derby, P.A. Sackinger, and P.D. Thomas, "Modelling of Czochralski crystal growth," *Proceedings of the Fifth Inter. Conf. on Numerical Methods in Thermal Problem*, (1987, in preparation).

25. M.J. Bennett, R.A. Brown, and L.H. Ungar, "Nonlinear Interactions of Interface Structures of Differing Wavelength in Directional Solidification," *Proceedings of the 1986 Inter. Symposium on the Physics of Structure Formation* (1987, in press).

Presentations (Since November 1985)

26. R.A. Brown, "Large-Scale Numerical Calculation Applied to Melt Crystal Growth," Department of Chemical Engineering, University of Michigan, Ann Arbor, December 1985.

27. R.A. Brown, "Nonlinear Analysis of Microscopic Pattern Formation in Directional Solidification," Department of Computer Science, Yale University, New Haven, February 1986.

28. R.A. Brown, "Large-Scale Computer Simulation of Microscopic Transport Phenomena in Materials Processing," Department of Chemical Engineering, University of California at Berkeley, Berkeley Lecture, Berkeley, March 1986.

29. R.A. Brown, "Models of Melt Crystal Growth," Department of Chemical Engineering, University of California at Berkeley, Berkeley, March 1986.

30. R.A. Brown, "Nonlinear Analysis of Transport Processes," Six Lecture Series, Department of Chemical Engineering and the Applied Mathematics Program, Princeton University, May 1986.

31. R.A. Brown, "Microscopic Pattern Formation in Directional Solidification," Department of Chemical Engineering, Cornell University, Ithaca, October 1986.

32. M.J. Bennett, R.A. Brown, and L.H. Ungar, "Transitions in Microscopic Melt/Solid Interface Morphologies During Directional Solidification," Invited paper at the SIAM Fall Meeting, Tempe, October 1985.

33. R.A. Brown and P.M. Adornato, "Convection, Segregation and Interface Morphology during Directional Solidification," AIChE Annual Meeting, Chicago, November 1985.

34. P.A. Sackinger and R.A. Brown, "Nonlinear Transitions in Natural Convection Inside a Cylinder Heated from Below," AIChE Annual Meeting, Chicago, November 1985.

35. R.A.Brown, M.J. Bennett, and L.H. Ungar, "Nonlinear Dynamics of Two-Dimensional Cellular Solidification," Invited paper at the Engineering Foundation Workshop on Partially Solidified Systems, Fallen Leaf Lake, May 1986.

36. R.A. Brown, "Overview of Process Modelling," Plenary lecture at the National Forum on the Forum on the Future of Automated Materials Processing in the United States, National Bureau of Standards, May 1986.

37. R.A. Brown and M.J. Bennett, "Chaotic Interaction of Shallow Cells During Directional Solidification," Tenth U.S. Congress of Applied Mechanics, Austin, June 1986.

38. D.-Y. Kim, P.M. Adornato, and R.A. Brown, "Prediction of Dopant Segregation and Melt/Solid Interface Shape for Vertical Bridgman Growth with a Vertical Magnetic Field," VII International Conference on Crystal Growth, York, July 1986.

39. M.J. Bennett and R.A. Brown, "Chaotic Interactions of Shallow Cells During Directional Solidification," VII International Conference on Crystal Growth, York, July 1986.

40. R.A. Brown, "Modelling of Convection and Mass Transport in Melt Crystal Growth," Invited Lecture at the 6th International Summer School on Crystal Growth," Edinburgh, July 1986.

41. R.A. Brown, "Transport Processes in Directional Solidification on Earth and in Microgravity," Invited Lecture at the 33rd Annual Meeting of American Astronautical Society, Boulder, October 1986.

Personnel

Dr. P.M. Adornato, Ph.D. from MIT, January 1986, With Mobil Research and Development Laboratory, Paulsboro, NJ.

Mr. J.L. Duranceau, in sixth year of study toward Ph.D. Primary developer of finite element analysis for floating zone system. Supported by NASA.

Mr. P. Sackinger, in fifth year of study toward Ph.D. Research into nonlinear transitions in buoyancy-driven convection. Partially supported by NASA.

Mr. M.J. Bennett, in fifth year of study toward Ph.D. Research into nonlinear dynamics of cellular solidification. Partially supported by NASA.

Mr. D.H. Kim, in third year of study toward Ph.D. Research into convection and segregation in vertical Bridgman growth. Partially supported by NASA.

Mr. John Lee, in second year of study toward Ph.D. Developer of experimental system for study of dynamics of solidification for two-dimensional cells. Primarily supported by NASA.